nature communications

Article

https://doi.org/10.1038/s41467-025-61111-7

Identification of RNF114 as ADPr-Ub reader through non-hydrolysable ubiquitinated ADP-ribose

Received: 15 January 2025

Accepted: 11 June 2025

Published online: 09 July 2025

Check for updates

Max S. Kloet[1,5], Chatrin Chatrin[2,5] ✉, Rishov Mukhopadhyay[1,5], Bianca D. M. van Tol[1], Rebecca Smith[2], Sarah A. Rotman[3], Rayman T. N. Tjokrodirijo[3], Kang Zhu[2], Andrii Gorelik[2], Lucy Maginn[2], Paul R. Elliott[4], Peter A. van Veelen[3], Dragana Ahel[2], Ivan Ahel[2] ✉ & Gerbrand J. van der Heden van Noort[1] ✉

Crosstalk between the post-translational modification processes of ubiquitination and ADP-ribosylation occurs in DNA-damage- and immune-responses, in addition the physical linkage of ADP-ribose and ubiquitin is found during bacterial infection. Here, we study the ubiquitination of ADP-ribose mediated by human Deltex E3 ligases and the subsequent fate of the formed hybrid post-translational modification. We prepare a non-hydrolysable ADPr-Ub probe that we employ in a proteomics approach and identify RNF114 as an interacting protein. Using biophysical and biochemical experiments, we validate that RNF114 preferentially interacts with ubiquitinated ADP-ribose over non-modified ubiquitin. Subsequently, RNF114 can elongate the ubiquitinated ADP-ribose with a K11-linked ubiquitin chain. Using domain deletion analysis, we pinpoint the tandem zinc fingers and ubiquitin interacting motif (ZnF2 + ZnF3+UIM) domains of RNF114 to be crucial for recognising ubiquitinated ADP-ribose. Moreover, these domains are essential for the recruitment of RNF114 to the sites of laser-induced DNA damage.

Ubiquitination is a much-studied post-translational modification (PTM) that plays crucial roles in regulating cellular processes across eukaryotes. Canonical ubiquitination relies on a cascade of E1-, E2-, and E3 enzymes which conjugate the Gly76 C-terminus of ubiquitin (Ub) to the lysine side chains in proteins creating a stable iso-peptide bond[1]. However, it became evident that Ub can also be conjugated to non-lysine residues in proteins to form a thioester bond with cysteine[2,3] or an oxyester bond with serine or threonine[4–6]. Beyond protein modification, recent discoveries reveal ubiquitination on several non-protein substrates, such as lipopolysaccharide[7], oligosaccharide[8], phosphatidylethanolamine[9], nucleic acids[10,11], as well as on another PTM; ADP-ribose (ADPr)[12,13].

ADP-ribosylation is an ancient modification which is conserved across all kingdoms of life. This modification relies on ADP-ribosyltransferase enzymes which utilize NAD^+ and transfer ADPr onto proteins and nucleic acids[14,15]. Crosstalk between ubiquitination and ADP-ribosylation occurs in mammals, where, for instance, poly-ADPr (PAR) chains direct subsequent ubiquitination events in DNA damage responses[16], Wnt signaling[17], and ADPr-dependent ubiquitination in immune responses[18]. Such crosstalk is also cleverly utilized by bacteria, which themselves lack Ub, to disrupt host Ub signaling by modifying it with ADPr, as shown for *Legionella* and *Chromobacterium*[19,20]. These are prime examples where the already complex ubiquitination code is made even more diverse upon crosstalk with ADPr.

[1]Department of Cell and Chemical Biology, Leiden University Medical Centre, Leiden, the Netherlands. [2]Sir William Dunn School of Pathology, University of Oxford, Oxford, UK. [3]Centre for Proteomics and Metabolomics, Leiden University Medical Centre, Leiden, the Netherlands. [4]Department of Biochemistry, University of Oxford, Oxford, UK. [5]These authors contributed equally: Max S. Kloet, Chatrin Chatrin, Rishov Mukhopadhyay.
✉e-mail: chatrin.chatrin@path.ox.ac.uk; ivan.ahel@path.ox.ac.uk; gvanderheden@lumc.nl

https://doi.org/10.1038/s41467-025-61111-7

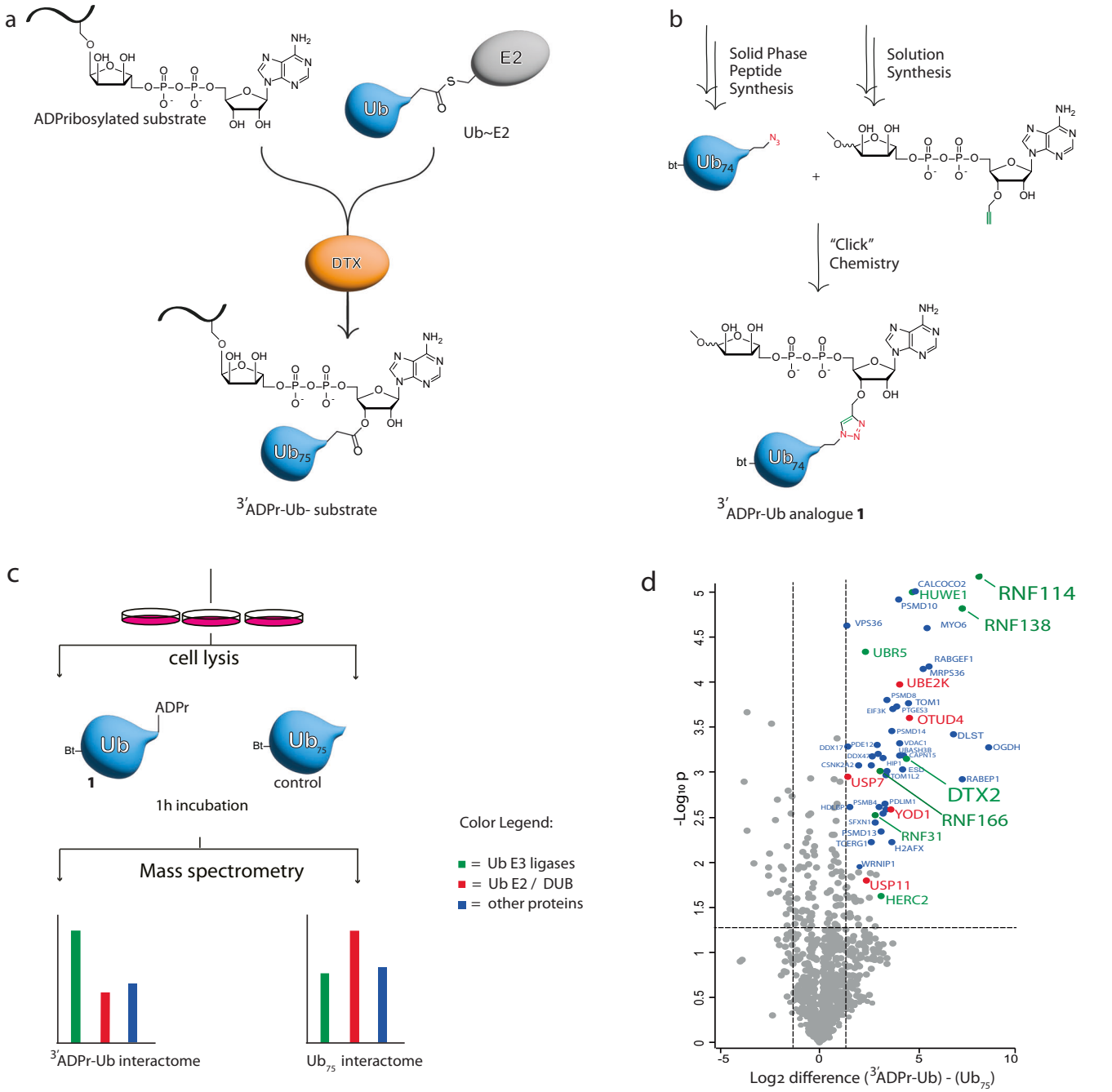

Fig. 1 | Quantitative proteomics identifies interactors of ADPr-Ub probe 1. **a** Schematic representation of the ubiquitin conjugation activity of DTX enzymes on ADP-ribosylated substrates. **b** Chemical synthesis scheme to obtain **1** via CuAAC between 3′-*O*-propargylated ADPr and bt-Ub bearing a C-terminal azide. **c** Schematic representation of the workflow for quantitative proteomics to identify proteins interacting with ADPr-Ub probe **1**. **d** Volcano plot showing the interactome of probe **1**. Data are normalized to the Ub_{75} interactome. Dotted lines represent significance and correspond to the thresholds: log2 ratio ≥ 1.3; *p*-value ≤ 0.05. A two-sided student's *t* test with permutation-based FDR was used to calculate the significance between probe and control at 0.05 FDR (*p*-value). Source data are provided as a Source Data file.

In humans, the family of Deltex RING E3 Ub ligases (DTX1, DTX2, DTX3, DTX3L, DTX4) catalyze Ub conjugation to the 3′-hydroxyl group of ADPr, which results in a hybrid ubiquitinated ADPr modification (further annotated as ADPr-Ub) (Fig. 1a)[12,13,21]. It was first reported that the heterodimeric complex of DTX3L/PARP9 conjugates ADPr to the Gly76 residue of Ub[22]. This unique reaction is catalyzed by all members of Deltex E3 ligases through their conserved RING and DTC domains, which interact with Ub-loaded E2 (E2-Ub) and NAD^+/ADPr, respectively[21]. The DTC domains of Deltex E3 ligases bind to NAD^+ and ADPr, and can recruit ADP-ribosylated proteins for ubiquitination[23]. However, instead of ADP-ribosylation of Ub, Deltex E3 ligases catalyze the ubiquitination of ADPr on the 3′-hydroxyl of adenosine ribose (Fig. 1a)[12]. To support these reactions, the DTC domains of Deltex E3 ligases harbor a conserved Glu-His diade to deprotonate the 3′-hydroxyl of the proximal adenosine ribose in ADPr to attack the thioester Ub-E2 conjugate, resulting in a covalent ester bond between Ub Gly76 and the ADPr 3′-hydroxyl group[12]. This allows the formation of a dual hybrid modification composed of ubiquitin and ADPr (ADPr-Ub) either on protein or nucleic acid substrates[12,13]. However, the biological function of such Deltex-catalyzed hybrid ADPr-Ub substrates remains unknown.

In this work, we wondered if there are proteins involved in reading this new expansion of the ubiquitin code, which would establish a first indication regarding the biological consequences and the underlying molecular mechanisms of the hybrid ADPr-Ub modification. One of the major challenges in studying the ADPr-Ub modification is the inherent lability of the ester bond. Here we synthesized a non-hydrolysable probe that mimics the formed ubiquitinated ADPr to perform an unbiased pulldown from cell lysate and start exploring its interactome. We identified RNF114 as one of the top binders for ADPr-Ub. RNF114 was previously suggested to bind mono-ADPr (MAR) and poly-ADPr (PAR) through its Zinc Finger (ZnF) domains[24,25]. We discovered that RNF114 mediates sub-micromolar binding to ADPr-Ub through its tandem ZnF2 + ZnF3 and Ub-interacting motif (UIM) domains. We further showed that RNF114 can engage ADPr-Ub and elongate it with K11-linked polyubiquitin chains, forming a novel mixed Ub chain linkage product. Finally, we show that the tandem ZnF2 + ZnF3 + UIM domains of RNF114 are responsible for its recruitment to the sites of DNA damage in cells, as we show that deletion of the RNF114 UIM or mutations in either the ZnF3 or UIM domain abolish recruitment to micro-irradiation sites. Combined this suggests that RNF114 is a reader of ADPr-Ub during response to DNA damage.

Results

Synthesis of an ADPr-Ub analogue

The activity of Deltex enzymes links the C-terminal Gly76 carboxylate of Ub to the 3′ proximal hydroxyl group of adenosine in ADPr or NAD^+, forming an ester bond. ADPr-esters have been shown to be chemically labile[26] and prone to acyl migration[27]. To prevent this and unwanted (enzymatic) hydrolysis when probing for interactors in cell lysate we envisioned a triazole linkage between ADPr and Ub to be the ideal stable linkage. Additionally, copper-catalyzed azide-alkyne cycloaddition (CuAAC) reactions between 1″-O-propargylated ADPr (distal ribose) and a Ub-mutant equipped with an azide on the Arg42 position were shown to be an effective method to install the ADPr moiety on Ub as the final step in synthesis, thereby reducing either acid or alkaline-induced problems during chemistry[28]. Considering these advantages, we here use a distinct connectivity between Ub and ADPr mimicking the ester linkage between the 3′-OH of ADPr and Gly76 of Ub. We introduced an azide-carrying ethane linker substituting the C-terminal Gly75 position in Ub and installed a propargyl functionality on the 3′-OH (proximal ribose) of ADPr. The synthesis of an ADPr-Ub analogue **1** was undertaken, establishing the inherently stable triazole linkage between Ub and ADPr (Fig. 1b). We used solid phase peptide synthesis to prepare the Ub protein and decorated the N-terminus with biotin (bt) to facilitate immobilization in pulldown experiments or detection of the probe in gel-based assays. After solid phase peptide synthesis, we installed an azido group via a short linker on the C-terminal tail of Ub. We introduced an alkyne on the 3′-alcohol of 1″-OMe-ADPr, a proxy of an ADP-ribosylated serine residue, by preparing a 3′-O-propargylated adenosine amidite that was conjugated to a suitably protected ribose-5″-O-phosphate via P(III)-P(V) methodology[29] (Supplementary Fig. 1). To facilitate the complete in-solution deprotection by aqueous ammonia, both fragments were protected with base-labile protecting groups. The successful CuAAC reaction joining the 3′-O-propargyl ADPr and bt-Ub-azide was followed by RP-HPLC purification to yield ADPr-Ub probe **1**.

Identification of ADPr-Ub readers using proteomics

In order to validate whether ADPr-Ub probe **1** can be used to profile the interactome of ubiquitinated ADPr we performed a pulldown from HEK293T cell lysate and immunoblotted against DTX2 (Supplementary Fig. 2). We confirmed DTX2 was enriched using probe **1,** whereas the negative control Ub_{75} was not able to enrich DTX2. Ub_{75} lacks both the ADPr moiety as well as the most C-terminal Gly76 residue, preventing it from being conjugated to substrates via the normal conjugation machinery. To identify relevant ADPr-Ub interactors in cells, a pulldown experiment using probe **1** was performed, including Ub_{75} as a negative control (Fig. 1c). Cells were lysed using CO-IP buffer and incubated with either probe or control, followed by biotin pulldown using Neutravidin beads. Pulldown samples were washed with CO-IP buffer under mild conditions and subjected to LC-MS/MS analysis. We normalized the data against proteins interacting with the Ub_{75} control and indeed could confirm the validity of this approach by identifying DTX2. Proteins most significantly interacting with probe **1** include RNF114 and RNF138, both Ub E3 ligases that have been linked to DNA damage repair pathways, regulation of ADP-ribosylation events, and immune responses[24,25,30–32] (Fig. 1d). Other interactors include OTUD4, USP7, YOD1 and USP11 reported as “erasers” of ubiquitination while interactors like UBR5, HUWE1, UBE2K, HERC2, RNF166 and RNF31 are reported as “writers” of ubiquitination. These proteins all exhibited a ≥1.3-fold difference in the Log_2 intensities and Log_{10} P value significance. Some of these hits (DTX2 and HUWE1) contain a WWE domain, which is reported to bind to the iso-ADPr moiety of PAR[33].

Although the volcano plot shows the difference in protein binding to ADPr-Ub compared to Ub_{75}, careful validation of the identified proteins as bona-fide dual modification (ADPr-Ub) interactors is warranted, as we cannot exclude the possibility that some of the found proteins bind to probe **1** due to changes in the biophysical parameters on the C-terminus of Ub, the artificial triazole linkage or to ADPr itself. For instance, a similar pull-down strategy using mono-ADPr has previously revealed DTX2 as an interactor of ADPr[34]. To demonstrate global variation among the three replicate samples and detect unknown patterns across various conditions, we employed principal component analysis (PCA). The PCA profile revealed clustering of replicates from different sample groups (Supplementary Fig. 3A). Furthermore, hierarchical clustering analysis demonstrated different protein interaction profiles for both probes (Supplementary Fig. 3B), where we highlighted the interaction profile of DTX2 and RNF114 (Supplementary Fig. 3C, D). Analysis of the ADPr-Ub interactome revealed multiple unique protein interactors of ADPr-Ub, including RNF114, RNF138, RNF166 and DTX2. Since RNF114, RNF138, and RNF166 are members of the same E3 ligase family, we decided to further investigate RNF114 as the most significant hit in the proteomics data as a representative family member.

RNF114 and DTX2 bind ADPr-Ub

We next investigated RNF114 as one of the most significant interactors from the proteomics data to verify bona-fide binding to biotin-ADPr-Ub probe **1** versus biotin-Ub and biotin-ADPr using immunoblotting. We also investigated DTX2, which was identified in our dataset and is one of the writers of ADPr-Ub modification[12,21]. For this experiment, the cell lysate was incubated with probe **1** and controls (biotin-Ub_{75} or biotin-ADPr). A pulldown with Neutravidin beads followed by immunoblotting indeed enriched both RNF114 as well as DTX2 by probe **1** and significantly less by both controls (Fig. 2a). Next, we sought to further validate the interaction between probe **1** and RNF114 and DTX2 using bio-layer interferometry (BLI) to determine their binding affinities. Both RNF114 and the truncated DTX2 Ring-DTC (RD) protein, the minimal protein identified as a writer of ADPr-Ub modification, show a strong interaction with ADPr-Ub but marginal binding to Ub or ADPr (Fig. 2c and Supplementary Fig. 4). Using a titration range, we were able to deduce apparent K_D's of 0.28 μM for RNF114 and 1.4 μM for DTX2-RD (Fig. 2c). Characterization of probe **1**, bt-Ub or bt-ADPr and RNF114 or DTX2-RD using the more sensitive Surface Plasmon Resonance (SPR) methodology confirmed the stronger interaction between RNF114 and DTX2-RD towards ADPr-Ub over Ub and ADPr only (Fig. 2b, c and Supplementary Figs. 5 and 6).

RNF114 elongates ADPr-Ub

Our results thus far suggest that RNF114 and DTX2-RD bind the dual ADPr-Ub modification more strongly than Ub or ADPr in isolation.

https://doi.org/10.1038/s41467-025-61111-7

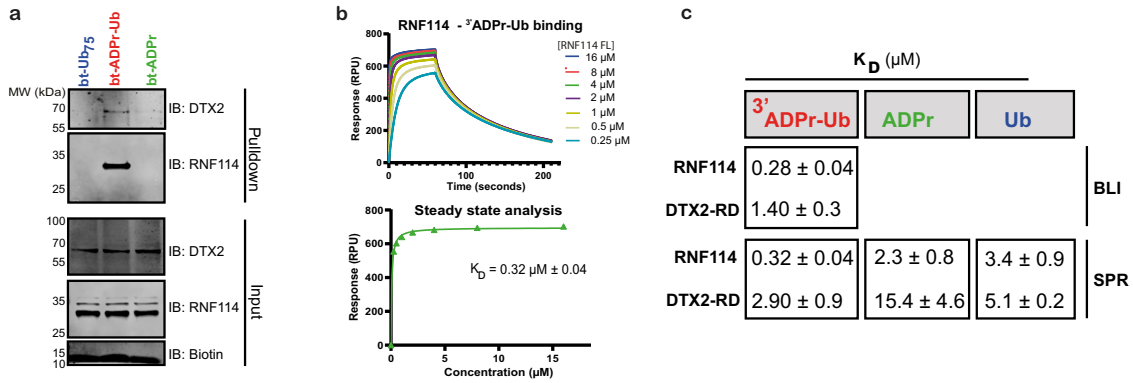

Fig. 2 | DTX2 and RNF114 interact with ADPr-Ub. a Cell lysate from HEK293T cells was incubated with biotin-ADPr-Ub probe **1**, biotin-Ub_{75} and biotin-ADPr (5 μM) and a pull down using Neutravidin beads was performed. Western blot shows levels of endogenous DTX2 and RNF114 (input) and pulldown confirms interacting with probe **1**. Source data are provided as a Source Data file. Representative blots for $n = 2$ independent experiments are shown. **b** SPR response curves and analysis of RNF114 to biotin-ADPr-Ub. **c** K_D binding affinities of RNF114 and DTX2 deduced from BLI and SPR measurements. Maximum concentration of RNF114 and DTX2-RD used in these assays were 16 μM and 40 μM, respectively. Source data are provided as a Source Data file.

While the RD domains of Deltex proteins, including DTX2, are able to catalyse Ub transfer to ADPr or NAD^+ in the presence of ubiquitination cascade components, the role of RNF114 in relation to ADPr-Ub is unclear. Unlike DTX2, RNF114 is unable to catalyse ADPr-Ub adduct formation when tested with ^{32}P-NAD^+ and ubiquitin cascade components (Fig. 3a, Supplementary Fig. 7A). To our surprise, when both DTX2-RD and RNF114 are present in the reaction, we noticed a formation of ladders consistent with ubiquitination on ^{32}P-NAD^+-Ub (^{32}P-NAD^+-Ub_n). A previous study reported that RNF114 efficiently catalyses the formation of polyubiquitin chains[35]. Indeed, we also observe that RNF114 forms free polyubiquitin chains in a time- and concentration-dependent manner (Supplementary Fig. 7B). We postulate that the ^{32}P-NAD^+-Ub_n ladders are generated as RNF114 transfers Ub onto existing ^{32}P-NAD^+-Ub catalysed by DTX2-RD. To verify this hypothesis, we tested both DTX2-RD and RNF114 in the presence of ubiquitin cascade components (E1/E2 (UbcH5B)/Ub/Mg^{2+}-ATP) and biotin-Ub or biotin-ADPr-Ub. In reactions with biotin-Ub, we observed auto-ubiquitination with DTX2-RD and the formation of Ub_2, Ub_3, and Ub_4 ladders with RNF114 (Fig. 3b, first group). Notably longer chains than Ub_4 are hardly formed and this seems to be the maximum limit of RNF114 under the used conditions. In reactions with biotin-ADPr-Ub, we only observe Ub_2, Ub_3, and Ub_4 formed with RNF114, and no DTX2 auto-ubiquitination (Fig. 3b, second group). RNF114 further prefers to catalyse Ub transfer to biotin-ADPr-Ub probe **1**, as opposed to biotin-Ub when followed over time, as is evident from the intensity of the tetra-Ub bond (Fig. 3c) or the remaining unanchored mono-Ub bands, with 16% remaining ADPr-Ub probe **1** and 70% remaining biotin-Ub after 30 min (Fig. 3d).

To investigate if ADPr-Ub elongation is unique to RNF114, we tested other E3 ligases for their ability to utilize ADPr-Ub as a substrate (Supplementary Fig. 8). Out of all the E3 ligases tested (RING E3s DTX2, DTX3L, RNF4, cIAP1, TRIM25, and HECT E3 Nedd4), only RNF114 was able to efficiently elongate ADPr-Ub. UbcH5B/Nedd4 generates (K63-linked) polyubiquitin chains on biotin-Ub but does not elongate biotin-ADPr-Ub. Using a different E2/E3 combination, UBE2N/UBE2V1/TRIM25, generates (K63-linked) polyubiquitin chains on biotin-Ub, but is less efficient in elongating biotin-ADPr-Ub. These data contrast with RNF114, which elongates biotin-ADPr-Ub more efficiently than biotin-Ub (Fig. 3c, d). Altogether, these results suggest that RNF114 is unique in its preference to elongate ADPr-Ub, compared to the other E3s tested here.

RNF114 elongates ADPr-Ub via K11 linkage

To understand how RNF114 elongates ADPr-Ub, we looked at the Alphafold-predicted structural model of RNF114 and how RNF114 binds to E2 and Ub (Fig. 4a, Supplementary Fig. 9). RNF114 is an active RING E3 ligase, which possesses three ZnF domains and a UIM domain in its C-terminus. The second and third ZnF domains were suggested as mono-ADPr or poly-ADPr readers[24,25], and the UIM domain could pull down ubiquitin chains[36]. We postulated the possibility that the RNF114 binds ADPr-Ub through the C-terminal ZnF2 + ZnF3 + UIM domains. We first modelled how RNF114 binds to E2 UbcH5B and Ub. The resulting model shows that the RING domain binds UbcH5B, and the UIM domain binds Ub(acceptor). The relative orientation of RING + ZnF1 and ZnF2 + ZnF3 + UIM domains changes to accommodate E2 and Ub binding. Interestingly, the Ub-tail in the model is pointing towards the tandem ZnF2 + ZnF3 domains of RNF114, where an ADPr-moiety is possibly accommodated. (Supplementary Fig. 9A, B). To model an incoming Ub donor, we then modelled in UbcH5B–Ub (PDB: 4V3L) to bind to the RING domain of RNF114, and in this scenario, the $UbcH5B^{K85}$–Ub^{Gly76} iso-peptide bond is poised towards the acceptor Ub^{K11} within a~7 Å distance. We also modelled all components (RNF114, UbcH5B, two Ub donors, ADP, five Zn atoms), which gives an identical prediction (Fig. 4a, right, Supplementary Fig. 9C, D). These models would predict that the RNF114 can elongate bound Ub with the K11 linkage type.

We first tested if RNF114 can build specific Ub chain linkage types in an unbiased manner. We utilised a mass-spectrometry-based assay to screen for the selectivity of UbcH5B-RNF114 for assembling Ub chains. This method relies on simultaneously incubating the E3 with eight synthetically prepared neutron-encoded mono-Ub acceptors, each having a distinguishable mass[37]. These acceptors possess only one amine position available for ubiquitination (M1, K6, K11, K27, K29, K33, K48 or K63), combined with a blocked C-terminus to prevent their use in subsequent ubiquitination events[35]. The donor Ub, on the other hand, contains a fully functional C-terminus and contains no amine positions, precluding its use as an acceptor in the reaction. Upon E1, E2 and E3 mediated di-Ub formation, each formed linkage type hence has a distinct mass, allowing direct detection and quantification of the formed chain types by mass spectrometry. Out of the eight simultaneously tested acceptors, RNF114 consumes Ub K11 most significantly and likewise, mainly K11-linked Ub_2 (92%) is formed as product over time, with K48-linked Ub_2 as minor side product (7%) (Fig. 4b, c, Supplementary Fig. 10). These findings are in line with literature reports showing that RNF114 can generate K11 polyUb chains[35].

We subsequently tested a panel of deubiquitinases (DUBs) for the removal of RNF114-catalysed poly-ubiquitination on biotin-ADPr-Ub probe **1** (Fig. 4d, Supplementary Fig. 11). We found that USP2 (a promiscuous DUB) and Cezanne (a K11 linkage-specific DUB) were able to

https://doi.org/10.1038/s41467-025-61111-7

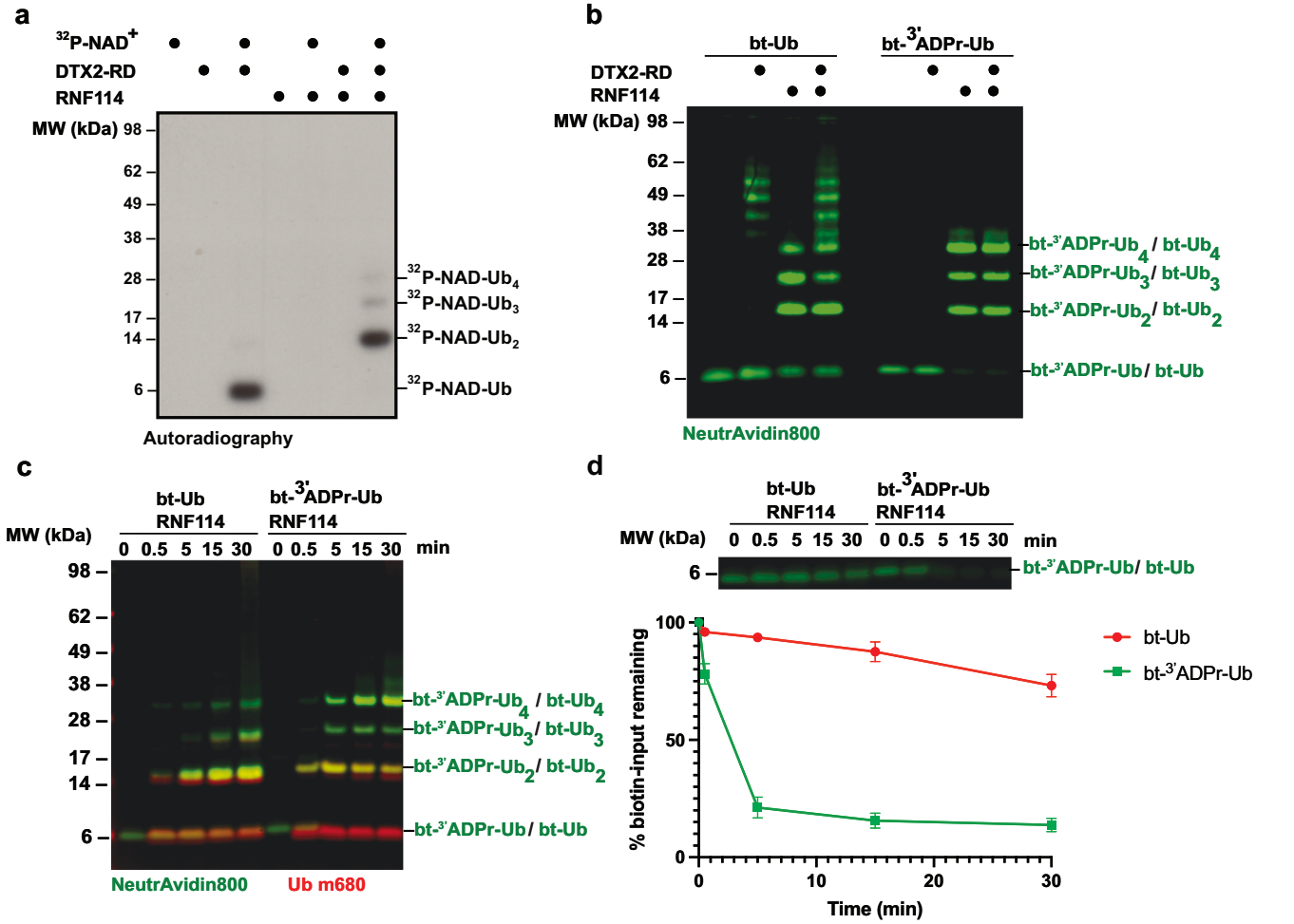

Fig. 3 | RNF114 elongates Ub chain on ADPr-Ub. a ^{32}P-NAD + -Ub formation assay with DTX2-RD and RNF114. RNF114 elongates Deltex-catalysed ^{32}P-NAD$^+$-Ub. **b** Ubiquitination assay using biotin-Ub and biotin-ADPr-Ub probe **1**. RNF114 elongates the Ub chain on biotin-Ub and biotin-ADPr-Ub probe **1**. **c** RNF114 elongates Ub chains in a time-dependent manner. Biotin signal is shown in green, and ubiquitin signal is shown in red. **d** Zoom-in on the decreasing levels of biotin-ADPr-Ub or biotin-Ub (top) and quantification of the remaining biotin signal (bottom). **a**–**d** All in the presence of E1/UbcH5B/Ub/Mg^{2+}-ATP. Data are presented as mean values ± SEM. For all experiments, two independent biological replicates were performed with similar results. Source data are provided as a Source Data file.

cleave all biotin-ADPr-Ub$_n$ signal as well as Ub$_n$ chains into mono biotin-ADPr-Ub. and mono Ub. OTUD2, a K11, K27, K29 and K33-linkage-specific DUB, showed weak removal activities, which reduces the poly-Ub cargo on Ub biotin-ADPr-Ub$_n$, although not completely. JOSD1 and OTULIN (a M1-specific DUB), and OTUB1 (a K48-specific DUB) did not remove the polyUb chain in these conditions. These results are consistent with our unbiased neutron-encoded Ub$_2$ formation assay and further suggest that RNF114 also elongates ADPr-Ub mainly through the K11 linkage.

RNF114 engages ADPr-Ub through its ZnF2 + ZnF3 + UIM domains

Next, we went on to validate the minimum RNF114 domains required for ADPr-Ub binding. The structural model suggested that RNF114 possibly binds ADPr-Ub through the ZnF2 + ZnF3 + UIM domains. To test this, we generated RNF114 domain truncations and tested their binding to the biotin-ADPr-Ub probe **1** using BLI (Fig. 5a, b, Supplementary Fig. 12). The loss of the UIM domain or mutations in the UIM domain resulted in ~25× worse affinity, whereas deletion of ZnF2 + ZnF3 + UIM domains resulted in a complete loss of detectable binding. The tandem ZnF2 + ZnF3 alone resulted in ~75× worse affinity compared to the full-length protein. Meanwhile, the ZnF2 + ZnF3 + UIM domains bind with 1.4 μM affinity, partially restoring the 280 nM affinity of the full-length protein. Together, these binding experiments suggest that ZnF2 + ZnF3 + UIM domains are the minimal module required for decent ADPr-Ub binding by RNF114.

We also tested the RNF114 truncations in Ub- and ADPr-Ub-elongation reactions. None of the truncations were able to elongate the Ub-chain to biotin-Ub or biotin-ADPr-Ub (Fig. 5c, Supplementary Fig. 13A). In an analogous set of experiments, we tested these truncations using DTX2-dependent ^{32}P-NAD$^+$-Ub with similar results (Fig. 5d, Supplementary Fig. 13B). Even ΔZnF2 + 3 + UIM and ΔUIM variants, which still contain the RING domain, were unable to elongate Ub or ^{32}P-NAD$^+$-Ub. This suggests that RNF114 requires both the RING domain and ZnF2 + 3 + UIM domains to elongate Ub and ADPr-Ub. Taking together these in vitro assays and binding experiment results indicate that RNF114 utilises its ZnF2 + ZnF3 + UIM domains to bind ADPr-Ub, which then elongates the Ub chain using its RING E3 ligase activity.

The model in Fig. 4a predicts a possible flexibility of the linker between the [RING + ZnF1] domain and the [ZnF2 + ZnF3 + UIM] domain, which dictates the relative orientation between the RING/bound E2–Ub(donor) and the [ZnF2 + ZnF3 + UIM] /bound Ub(acceptor). Besides this linker, the ZnF3- and UIM-domain are also connected via a short linker. We tested if altering the linker region between ZnF3 and UIM, or between ZnF1 and ZnF2, affects RNF114 activity (Fig. 5e, f). For each linker, we made either Gly/Ser substitution (keeping the same linker length) or introduced Gly/Ser insertion (increasing the linker length by 4 aa residues). Alterations in the linker between ZnF3 and

https://doi.org/10.1038/s41467-025-61111-7

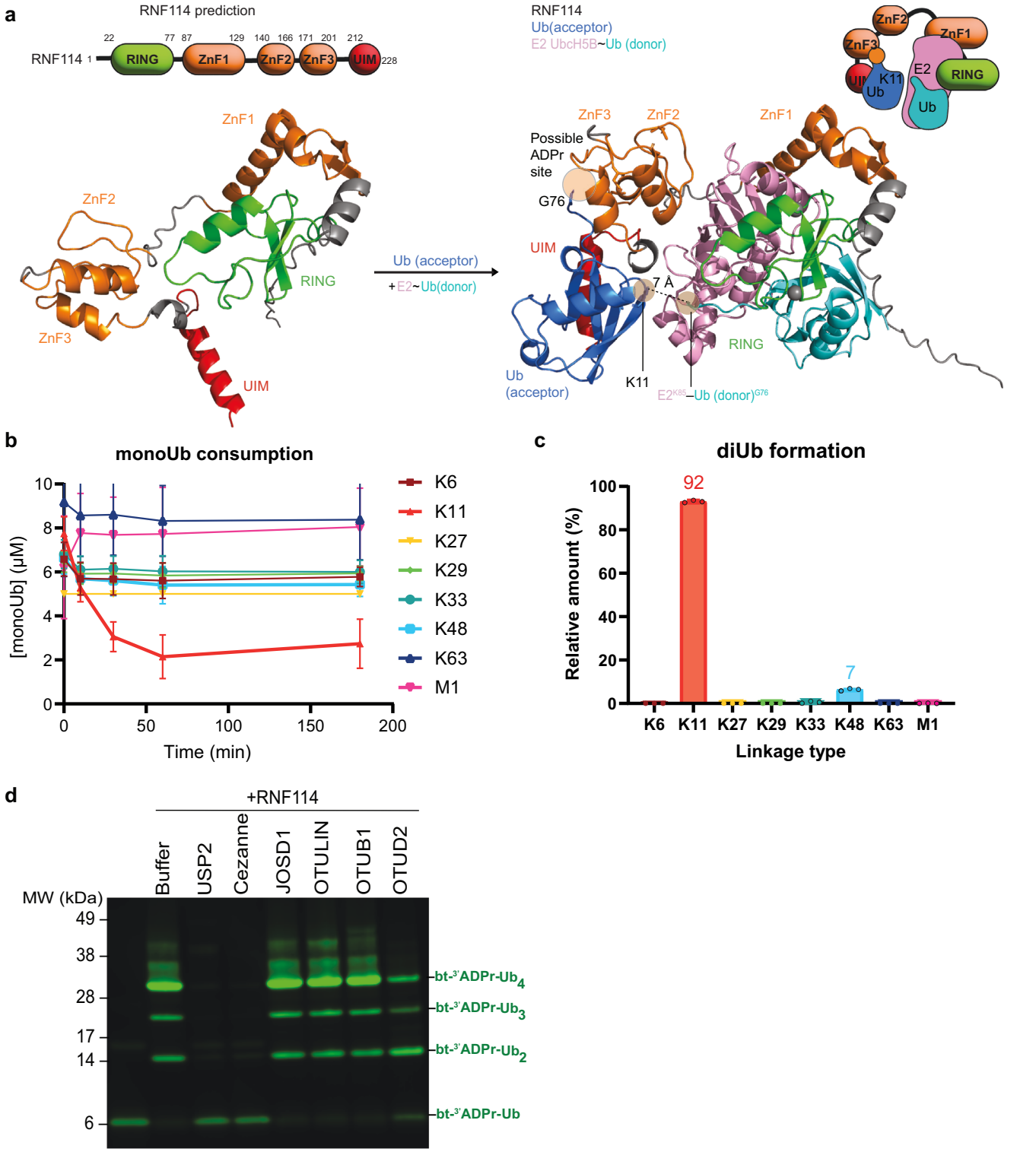

Fig. 4 | RNF114 elongates ADPr-Ub via K11 linkage. a Predicted structural model of RNF114 bound to acceptor Ub and UbcH5B–Ub. The donor UbcH5B^{K85}–Ub^{Gly76} isopeptide bond is poised towards the acceptor Ub^{K11}. Detailed description of how the model is obtained is available in Supp. Fig. 9. RNF114 prefers to elongate Ub on K11, as shown by neutron encoded mono-Ub consumption (**b**) and di-Ub formation (**c**). Data are presented as mean values of $n = 3$ independent experiments ± SEM. **d** Panel of DUBs remove RNF114-catalysed poly-ubiquitination on biotin-ADPr-Ub probe **1**. USP2 (a specific DUB) and Cezanne (K11-specific DUB) cleave the poly-ubiquitinated species completely, while OTUD2 shows minor DUB activity. Two independent experiments were repeated with similar results. Source data are provided as a Source Data file.

UIM were detrimental to RNF114's ability to elongate biotin-Ub and biotin-ADPr-Ub. Additional flexibility on the linker between ZnF1 and ZnF2 also led to 40–60% reduction in biotin-Ub and biotin-ADPr-Ub elongation, albeit better-tolerated. These results suggest that both the linkers between ZnF3–UIM and ZnF1–ZnF2 are important elements for RNF114's ability to elongate Ub and ADPr-Ub. In particular, the ZnF3-UIM linker holds a crucial role for anchoring the acceptor Ub. These effects are specific to Ub and ADPr-Ub elongation, as the linker mutations did not affect RNF114 auto-ubiquitination activity. These results suggest that the UIM domain is not only involved in the binding

https://doi.org/10.1038/s41467-025-61111-7

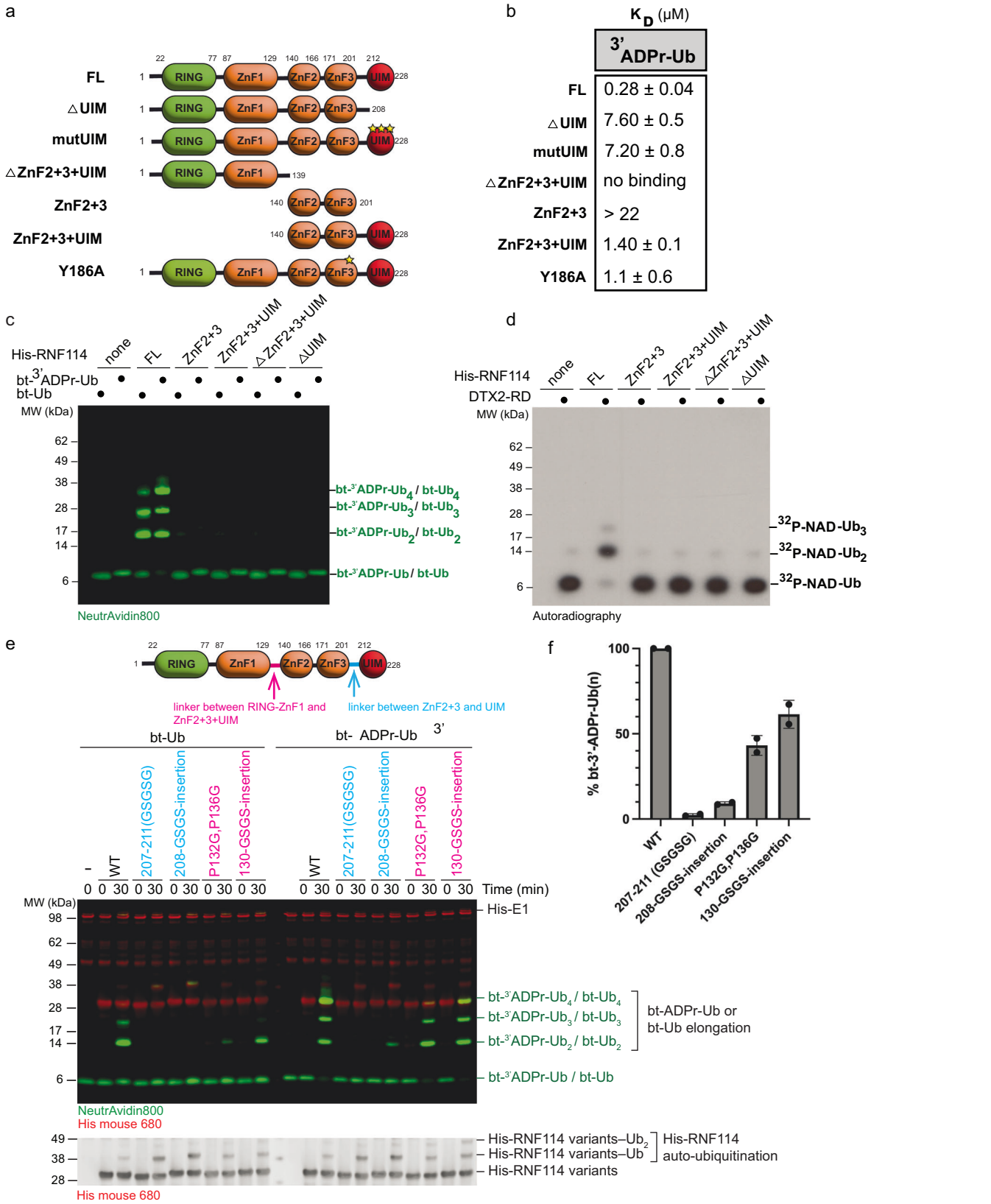

Fig. 5 | RNF114 ZnF2 + ZnF3 + UIM domains are responsible for ADPr-Ub binding and elongation. a RNF114 domain organisation and truncations and mutations used in this study. **b** Binding affinities of RNF114 truncations and mutants to biotin-ADPr-Ub probe **1** determined using Bio-Layer Interferometry. **c** Ub elongation reactions of biotin-ADPr-Ub probe **1** or biotin-Ub in vitro using RNF114 truncations and mutants. **d** ^{32}P-NAD$^+$-Ub in vitro elongation reactions with RNF114 truncations and mutants. **e** Ub elongation reactions of biotin-ADPr-Ub probe **1** or biotin-Ub using RNF114 linker mutations as indicated. **f** Quantification of biotin-ADPr-Ub$_{(n)}$ normalized to RNF114 WT. Data are presented as mean values ± SEM. For all experiments, two independent biological replicates were performed with similar results. Source data are provided as a Source Data file.

https://doi.org/10.1038/s41467-025-61111-7

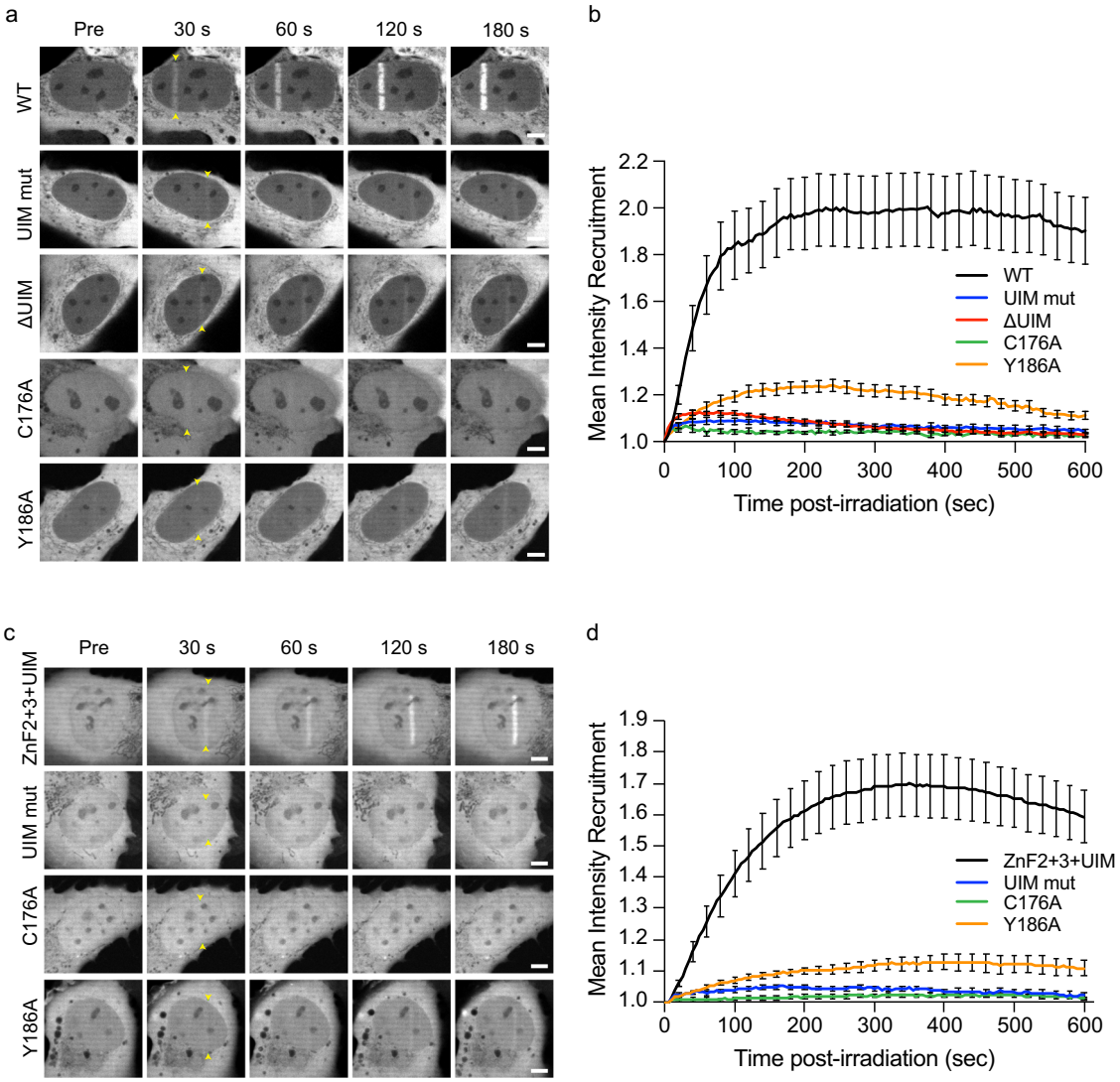

Fig. 6 | RNF114 recruitment to sites of DNA damage is dependent on its tandem ZnF2 + ZnF3 + UIM domains. a Representative images of YFP-RNF114 FL or truncations and mutants recruitment to sites of DNA damage induced by 405 nm irradiation in U2OS WT cells. Arrow heads indicate the site of damage. Scale bar, 5 μm. **b** Recruitment kinetics of YFP-RNF114 WT (Black), UIM mutant (Blue), ΔUIM (Red), C176A (green) or Y186A (Orange) to sites of damage. **c** Representative images of YFP-RNF114 ZnF2 + 3 + UIM WT or mutants recruitment to sites of DNA damage induced by 405 nm irradiation in U2OS WT cells. Arrow heads indicate the site of damage. Scale bar, 5 μm. **d** Recruitment kinetics of YFP-RNF114 ZnF2 + 3 + UIM (Black), UIM mutant (Blue), C176A (green) or Y186A (Orange) to sites of damage. Data are representative of three independent biological replicates. Curves show mean ± s.e.m. of at least 14 cells per condition. Source data are provided as a Source Data file.

or recruitment of Ub(acceptor), but also for its precise positioning for further elongation.

RNF114 recruitment to sites of DNA Damage Response sites in vivo is dependent on ZnF2 + 3 + UIM domains

Previous studies have shown that RNF114 is recruited to the sites of DNA damage either through mono-ADPr or poly-ADPr recognition by its ZnF2 + 3 domain[24,25], or through Ub recognition by the UIM domain[38], independently. Since we identified that ZnF2 + 3 + UIM domains of RNF114 are an ADPr-Ub binding module, we wondered if RNF114 recruitment to DNA damage sites is dependent on these domains. Based on the model obtained in Fig. 4a, the helical UIM domain is predicted to engage the hydrophobic I44 patch of Ub, and the ZnF3 domain can accommodate ADP binding (Supplementary Fig. 14). Based on this model, we generated full-length YFP-RNF114 with mutations on the UIM (V220G, L221G, S224G) or the ZnF3 (C176A or Y186A) domains that are predicted to impair Ub and ADPr binding, respectively. For RNF114 UIM domain, the hydrophobic V220 and L221 residues are well-conserved in other paralogues (RNF125, RNF138, and RNF166), while S224 is identical in all paralogues. These residues line the UIM helical face that contacts Ub I44 patch. For ZnF3 domain, C176 mutation will destabilise Zn finger fold, and Y186 which is also present in RNF166 is predicted to stack with the adenine ring of ADP. Interestingly, analogous tyrosine provides a critical interaction to ADPr in PAR-binding zinc finger domains of APLF and CHFR[39,40].

We compared the recruitment of these mutants to laser-induced DNA damage (Fig. 6, Supplementary Fig. 15). We found that these mutations significantly impair RNF114 recruitment to the sites of damage. Deleting the UIM domain also abolishes RNF114 recruitment to the damage sites, which suggests that RNF114 localisation to damage sites does not solely depend on the ADPr signal but also relies on the Ub signal. These ZnF3 and UIM mutants show 3-fold and 25-fold weaker binding to biotin-ADPr-Ub probe **1** as determined using BLI, respectively (Supplementary Fig. 16). These data underscore a previous finding that RNF114 relies on both the

UIM and ZnF2 + ZnF3 domains for its recruitment to DNA damage sites[38], and that this is likely to be driven by the dual ADPr-Ub signal.

Discussion

Ubiquitination of non-protein substrates is an emerging theme. However, investigating their biological function is challenging due to the lack of tools. The synthesis of non-hydrolysable ADPr-Ub analogue **1** allowed us to identify RNF114 in an unbiased manner as a reader of this recently discovered modification. The tandem ZnF2 + ZnF3 + UIM domains of RNF114 bind the ADPr-Ub probe with an affinity below 1 μM. This is surprisingly high, considering that UIM domains typically bind Ub with low affinity[41]. For Ub-binding domains, tighter binding and linkage selectivity is usually achieved through the arrangement of multiple domains to achieve linkage-specific avidity[42]. Our data suggest that RNF114 achieves tight ADPr-Ub binding due to having an adjacent ADPr-binding ZnF2 + ZnF3 domain and an Ub-binding UIM domain. It will be interesting to see if there are other proteins with adjacent ADPr-reader and Ub-reader functions that confer similar ADPr-Ub binding ability.

RNF114 is an E3 ligase that contains a C3HC4-type RING finger domain to support this function. Our biochemical reconstruction and structural modelling demonstrate that the ADPr-Ub binding modules cooperate with the RING domain to produce a novel mixed Ub linkage product, K11-linked ADPr-Ub_n. Also, the ability of RNF114 to elongate ADPr-Ub fits nicely with recent findings observed by other research groups. For example, DTX1/2/4 were reported to interact with PARylated TNKS1, which led to the stabilisation of mono-Ub TNKS1. RNF114 and its paralogue RNF166 interact with this mono-Ub TNKS1 and promote its K11-linked di-ubiquitination[32]. In particular, the tandem ZnF2 + ZnF3 + UIM domains were sufficient to stabilise mono-Ub TNKS1 species; these are the same domains identified in our study as ADPr-Ub binder. Our findings offer an explanation to complement these observations: that the DTX1/2/4-dependent mono-Ub TNKS1 species is possibly TNKS1-($3'$ADPr-Ub). RNF114, as well as RNF138 and RNF166, which come forward as significant binders to probe **1** in our proteomic data have been identified previously as binders of this ADPr transferase TNKS1[32]. Another recent study reported ubiquitination on mono-ADP-ribosylated PARP10 and shows that this can be extended with K11-linked chains[43]. It is highly possible that this K11-linked elongation is mediated by RNF114 or other paralogues within this E3-family found in human cells, such as RNF166, RNF138 or RNF125 all of which possess ZnF2 + ZnF3 + UIM domains in their C-terminus (Supplementary Fig. 14), although their ability to engage ADPr-Ub remains to be experimentally validated. These two examples indicate that ADPr-Ub modification on a substrate is uniquely recognised and has distinct biological outcomes. It remains to be seen if there are other possible substrates and fates for ADPr-Ub modification besides K11-linked elongation by RNF114.

Previously, it was shown that RNF114 is recruited to DNA damage in an ADP-ribosylation-dependent manner, which could be either a mono-ADPr or poly-ADPr-signal[24,25]. Another recent report showed that RNF114 recruitment to the sites of DNA damage is dependent on its UIM domain[38]. Excitingly, our data demonstrate that RNF114 recruitment to DNA damage sites relies on both the ZnF2 + ZnF3 and UIM domains. Paired with our identification of RNF114 as a tight ADPr-Ub binder, this strongly suggests that the UIM and ZnF2 + ZnF3 domains act as a specific dual reader module for the ADPr-Ub signal. We propose that RNF114 recruitment to damage sites is dependent on the hybrid ADPr-Ub signal, instead of separate ADPr or Ub modifications. It is known that upon DNA damage PAR and MAR signals are heavily induced, which can be ubiquitination targets of Deltex E3 ligases[10,12,13]. Moreover, ADP-ribosylation-dependent ubiquitination was also observed under interferon stimulation and this signal is dependent on both PARP14 and DTX3L/PARP9[18], the latter complex being an ADPr-Ub writer. This suggests that there might be a higher level of ADPr-Ub-substrate modification under such conditions. Although more labile compared to lysine ubiquitination, ester-linked ubiquitination has a cellular half-life of at least 1 h[44] in which the signal has the opportunity to be recognised and potentially drive biological outcomes.

In this work, we synthesised a non-hydrolysable ADPr-Ub analogue and identified RNF114 as the first reader of the dual ADPr-Ub modification. The development of chemical tools, such as Ub-PAR analogues, might facilitate the identification and characterisation of other readers of these non-canonical Ub codes. Our findings also open up the possibility to utilise RNF114 ZnF2 + ZnF3 + UIM domains to stabilise endogenous ADPr-Ub-substrates and identify them. For example, by using this as an enrichment strategy to preserve the labile ester-linked ADPr-Ub modification and combine it with an ester-compatible proteomics workflow[26] to identify ADPr-Ub-substrates and the sites of modification by MS. We also showed that the ADPr-Ub signal can be elongated by an enzyme that possesses both the reader module and the catalytic RING domain, like RNF114. This reveals the possibility of further Ub modification of an existing ADPr-Ub signal on a substrate. The recruitment of RNF114 to DNA damage sites suggests that ADPr-Ub may be an underappreciated signalling molecule in DNA damage response. As such, the ADPr-dependent E3 ligase activity of RNF114 was postulated to be the major contributor in regulating PARP1 ubiquitination and degradation by the proteasome. Inhibition of RNF114 using the natural product nimbolide was reported to impair breast cancer cell proliferation[45] and induce PARP1 trapping, which might open therapeutic potential in treating *BRCA*^{mut} cancers[25]. Yet, the role of the ADPr-Ub modification formed by RNF114 in DNA damage response and the specific DNA damage that triggers the recruitment, as well as spatio-temporal regulation, will require further clarification by future studies. On a related note, interferon stimulation induces ubiquitination foci that are dependent on ADP-ribosylation[18,46]. While revising this manuscript, three groups reported the potential ubiquitination of ADP-ribosylated substrate proteins, including PARP7 and Tankyrase1 by Deltex proteins[47–49]. This further substantiates that studying the hybrid ADPr-Ub signal under these biological conditions will potentially also uncover novel pathways in eukaryotic cells relying on the dual ADPr-Ub modification.

Methods

Cell culture

HEK293T (Cat# ATCC® CRL-3216™) cells were cultured in Dulbecco's modified Eagle's medium (DMEM) (Gibco). Medium was supplemented with 8% FCS. Cells were grown at 37 °C in a humidified 5% CO_2 incubator. All cell lines have been routinely tested for mycoplasma.

Cloning and plasmids

The constructs described in this paper were generated using standard polymerase chain reaction and verified by Sanger sequencing. For *E. coli* expression, RNF114 was cloned into pRSF Duet vector with an N-terminal 6x-His tag followed by a TEV cleavage site. Mutants were generated using QuikChange (Agilent) or Q5 (NEB) site-directed mutagenesis. For laser irradiation experiment, RNF114 variants with flanking attB1/attB2 sequence were cloned into a gateway cloning-compatible system (pDONR221 and pDEST N-terminal YFP).

Protein expression and purification

Proteins were expressed in *E. coli* Rosetta (DE3) cells. Cultures were grown in LB medium with appropriate antibiotic at 37 °C until they reached an OD_{600} of 0.6–0.8, then protein expression was induced by supplementing 0.2 mM isopropyl- β-D-1-thiogalactopyranoside at 18 °C for 16–18 h. Cells were harvested and resuspended in buffer A (50 mM Tris-HCl pH 8.0, 200 mM NaCl, 20 mM imidazole, 5 mM β-mercaptoethanol) and supplemented with 0.2 mM phenylmethylsulfonyl fluoride. The resuspended cells were lysed using

homogeniser at 15,000 psi and cleared by high-speed centrifugation at 39,800 × *g* for 1 h at 4 °C. The cleared lysate was incubated with Ni^{2+}-NTA resin or HisTrap FF column (Cytiva), washed in buffer A, and eluted in buffer B (50 mM Tris-HCl pH 7.5, 200 mM NaCl, 200 mM imidazole, 5 mM β-mercaptoethanol). Eluted proteins were further purified by size exclusion chromatography on a Superdex 200 column (Cytiva) pre-equilibrated in 20 mM HEPES pH 7.5, 150 mM NaCl and 1 mM DTT. Fractions of interest were checked on SDS-PAGE, pooled, and concentrated on Amicon protein concentrator device (Merck Millipore). Protein concentrations were determined by A280 measurement using a nanodrop device and calculated using predicted molar extinction coefficients. Proteins were kept in aliquots, snap-frozen in liquid nitrogen, and stored in −70 °C. His-E1, UbcH5B, His-DTX2-RD, His-DTX3L-RD, RNF4, cIAP1, Nedd4, TRIM25, USP2, Cezanne, JOSD1, OTULIN, OTUD2, OTUB1 were generated as previously described[10,12,21,50].

In vitro assays

RNF114 Ub chain formation assay. Reactions were performed in 50 mM Tris-HCl pH 8.0, 50 mM NaCl, 2.5 mM $MgCl_2$, 2.5 mM ATP, 0.2 μM His-E1, 2 μM UbcH5B, 20 μM Ub, and the indicated RNF114 concentration at 37 °C for up to 1 h. Reactions were stopped by adding 4× LDS and 100 mM DTT. Samples were loaded onto SDS-PAGE (4-12% Bis-Tris gel/MES buffer) and visualised by Instant Blue stain.

^{32}P-NAD$^+$-Ub elongation assay. Reactions were performed in 50 mM Tris-HCl pH 8.0, 50 mM NaCl, 2.5 mM $MgCl_2$, 2.5 mM ATP, 0.2 μM His-E1, 2 μM UbcH5B, 20 μM Ub, 1 μM DTX2-RD, and 40 μM NAD^+ spiked with 40 nCi/μL ^{32}P-NAD^+ at 37 °C for 30 min to generate ^{32}P-NAD^+-Ub. To initiate elongation, 1 μM His-RNF114 (FL or variants) was added and incubated at 37 °C for 30 min. Reactions were stopped by adding 4× LDS and 100 mM DTT. Samples were loaded onto SDS-PAGE (4–12% Bis-Tris gel/MES buffer) and visualised by autoradiography.

Biotin-ADPr-Ub analogue elongation assay. Reactions were performed in 50 mM Tris-HCl pH 8.0, 50 mM NaCl, 2.5 mM $MgCl_2$, 2.5 mM ATP, 0.2 μM His-E1, 2 μM UbcH5B, 20 μM Ub, 10 μM biotin-ADPr-Ub, and 1 μM His-RNF114 (FL or variants) at 37 °C for 30 min. For E3 ligases screen, 1 μM of the indicated E3 ligases were used instead of His-RNF114. For Fig. 3b, c, either 10 μM biotin-Ub or biotin-ADPr-Ub were added as indicated. For samples treated with DUBs (Fig. 4d), reactions were stopped with 50 mM EDTA, followed by addition of 1 μM DUBs and further incubation at 37 °C for 30 min. Reactions were stopped by adding 4× LDS and 100 mM DTT. Samples were loaded onto SDS-PAGE (4–12% Bis-Tris gel/MES buffer), transferred onto nitrocellulose membrane (Biorad TransBlot Turbo), and blocked with 5% BSA. The membrane was incubated with primary antibodies (mouse monoclonal anti-Ub(PD41), Santa Cruz Biotechnology sc-8017, or 6xHis mouse monoclonal antibody, Takara #631212) overnight at 4 °C followed by secondary Li-Cor goat-anti mouse IRDye 680 and NeutrAvidin800 antibodies (Thermo Fisher). Membranes were washed in 0.1% PBS-Tween 20 (PBST) and scanned using Li-Cor Odyssey CLx imager.

Modelling. Structural prediction of RNF114 was obtained from Alphafold 3 (AF-Q9Y508-F1-v4).

Prediction of RNF114 bound to Ub(acceptor) and E2 UbcH5B were obtained using AlphaFold2 Multimer/ColabFold and AlphaFold3[51–53]. The Ub(donor) was modelled in using a structure of UbcH5B–Ub bound to RNF38 (PDB: 4V3L), by aligning the Cα of both UbcH5B (RMSD = 0.68 over 144 residues). The resulting model shows the $UbcH5B^{K85}$–Ub^{Gly76} isopeptide bond is poised towards the acceptor Ub^{K11} within a ~7 Å distance, which is shown in Fig. 4a. Structural figures were prepared in PyMOL (Schrodinger). Predicted aligned error (PAE) plots were visualised using PAE Viewer[54].

SDS-PAGE and immunoblotting. Samples were resolved on precast Bis-Tris NuPAGE gels (Invitrogen, 4–12%, 12%). MOPS buffer (Invitrogen Life Technologies, Carlsbad, USA) for Bis-Tris gels was used as running buffer. Proteins were transferred to a nitrocellulose membrane (Protran BA85, 0.45 μm, GE Healthcare) at 300 mA for 2.5 h. The membranes were blocked in 5% milk (skim milk powder, LP0031, Oxiod) in 1× PBS (P1379, Sigma-Aldrich), incubated with a primary antibody diluted in 5% milk in 0.1% PBS-Tween 20 (PBST) overnight, washed three times for 10 min in 0.1% PBST, incubated with the secondary antibody diluted in 5% milk in 0.1% PBST for 30–45 min, and washed three times again in 0.1% PBST. Immunoblot signals were visualized with a LI-COR Odyssey Fx laser scanning fluorescence imager and analyzed using LI-COR Image Studio Lite software.

For Supplementary Fig. 15, U2OS cells were plated in 6-well plates and transfected with RNF114-YFP plasmids and YFP as a control (TransIT-LT1 Transfection Reagent (Mirus Bio). 24 h after transfection cells were washed in Dulbecco's Phosphate Buffered Saline, scraped and centrifuged at room temperature to obtain pellets. Pellets were lysed immediately by resuspension in 60 μl lysis buffer (50 mM Tris pH 8, 100 mM NaCl, 1% Triton X-100 pH 8, protease and phosphatase inhibitor, 1 μM olaparib, 1 μM PARG inhibitor (PDD00017273, Sigma Aldrich), 2 μM benzonase) and incubated on ice for 30 min to extract proteins. Protein concentration was determined using the Pierce™ BCA Protein Assay Kit (ThermoFisher Scientific, #23225) according to the manufacturer's instructions and adjusted to 1 μg/μl by adding the required volume of MilliQ H_2O and NuPAGE® 1X LDS Sample Buffer (ThermoFisher Scientific) with a final concentration of 25 mM DTT. Samples were then boiled at 95 °C for 3 min. Samples were loaded on a NuPAGE™ 4–12% Bis-Tris Gels (Invitrogen). Gels were subsequently subjected to SDS-PAGE at 160 V in MOPS buffer before transfer to a Trans-Blot Turbo Transfer membrane (Bio-Rad) using a Trans-Blot Turbo Transfer System (Bio-Rad) (standard 30 min transfer). Ponceau S staining (Sigma) was used to determine transfer efficiency. Membranes were blocked using 5% (w/v) bovine serum albumin (BSA) in 1X phosphate-buffered saline-0.1% (w/v) Tween® 20 (PBS-T) for 1 h. Membranes were subsequently incubated with primary antibodies overnight at 4 °C, followed by washing with PBS-T and secondary antibody incubation for 1 h at room temperature. After washing the membranes with PBS-T, the blots were visualized using the Odyssey CLx Imager (LI-COR Biosciences). Quantification was performed using the Odyssey Image Studio Lite® software v.5.2 (LI-COR Biosciences).

Antibodies. Primary antibodies used for the study were: mouse anti-DTX2 (ProteinTech, #67209-1-Ig), rabbit anti-RNF114/ZNF313 (Invitrogen, #PA5-98120), mouse anti-Ub (Santa Cruz Biotechnology, sc-8017), alpha-tubulin (ProteinTech, 11224-1-AP), GFP (Santa Cruz Biotechnology, sc-9996). Secondary antibodies used were: IRDye 800CW goat anti-rabbit IgG (H + L) (Li-COR, Cat# 926-32211, 1:5000), IRDye 800CW goat anti-mouse IgG (H + L) (Li-COR, Cat# 926-32210, 1:5000), goat anti-mouse IgG secondary (680RD, 926-68070, Li-COR, 1:20000), Neutravidin protein, DyLigtht™ 800 (Thermo Fisher #22853), alpha-tubulin (Proteintech, 11224-1-AP, 1:5000, rabbit), GFP (Santa Cruz, sc-9996, 1:2000, mouse), goat anti-rabbit IgG secondary (800CW, 926-32211, Li-COR Biosciences, 1:20000), goat anti-mouse IgG secondary (680RD, 926-68070, Li-COR Biosciences, 1:20000). All antibodies were diluted in 5% (w/v) BSA in 1X PBS-T.

Pull-down assays. For pull-down, the medium was completely removed from the cells, followed by the addition of 300 μL lysis/co-IP buffer (50 mM TRIS, 150 mM NaCl, 0.8% NP40, Roche Protease inhibitor) and scraping of the cells. Samples were prepared in triplicates ($n = 3$) for pull-down using probe **1** and control Bt-Ub_{75}. Cell lysis was done as described above. The supernatant was transferred to a new Eppendorf tube. 15–20 μL of supernatant was removed to blot for the input sample. The remaining supernatant was incubated with a probe

(diluted in the same buffer to a final concentration of 5 μM) for 60 min at 37 °C. Next, the total volume was completed to 1 mL with the lysis buffer. 30 μL of Neutravidin beads (Thermo Scientific™, Pierce™ NeutrAvidin™ Agarose, Catalog number: 29,200) were added, followed by incubation at 4 °C on rollers overnight. Beads were collected by centrifugation at 500 x *g* for 1 min at 4 °C and washed with wash buffer (50 mM TRIS, pH 7.5, 150 mM NaCl, 0.5% Triton X, 0.5% SDS) at least 3 times by centrifuging at 500 x *g* for 1 min at 4 °C. Prior to the final washing, beads were transferred to a new tube to avoid background and finally centrifuged at 500 x *g* for 3 min at 4 °C. Beads and supernatant were stored at −80 °C until following analyses, including immunoblotting, fluorescent scanning, Coomassie staining and LC/MS-MS.

Processing of protein gel bands. For MS analysis, samples (3 replicates per condition) were put on a gel and run into the gel for 1 cm, and stained with SimplyBlue Coomassie safe stain. Each lane was cut into 4 bands. Gel slices were washed with 50 mM ammonium bicarbonate pH = 8.4 (AMBIC), subjected to reduction with 10 mM dithiothreitol in AMBIC, and alkylation with 55 mM of iodoacetamide in AMBIC. After 3 shrink/wash cycles (pure acetonitrile/AMBIC) 30 μL of 12.5 ng/μL trypsin was added for digestion, which took place at 37 ° overnight. All steps were performed in the Proteineer DP digestion robot (Bruker). Tryptic peptides were extracted from the gel slices with 50% acetonitrile in water with 1% formic acid and lyophilized.

Mass spectrometry. Peptides were dissolved in water/formic acid (100/0.1 v/v) and analyzed by online C18 nanoHPLC MS/MS with a system consisting of an Ultimate3000nano gradient HPLC system (Thermo, Bremen, Germany), and an Exploris480 mass spectrometer (Thermo). Samples were injected onto a cartridge precolumn (300 μm × 5 mm, C18 PepMap, 5 um, 100 A, and eluted via a homemade analytical nanoHPLC column (50 cm × 75 μm; Reprosil-Pur C18-AQ 1.9 um, 120 A (Dr. Maisch, Ammerbuch, Germany). The gradient was run from 2 to 40% solvent B (20/80/0.1 water/acetonitrile/formic acid (FA) v/v) in 30 min at 250 nL/min. The nano-HPLC column was drawn to a tip of ~10 μm and acted as the electrospray needle of the MS source. The mass spectrometer was operated in data-dependent MS/MS mode, with an HCD collision energy at 30% and recording of the MS2 spectrum in the orbitrap, with a quadrupole isolation width of 1.2 Da. In the master scan (MS1) the resolution was 120,000, the scan range 400–1500, at standard AGC target and a maximum fill time of 50 ms. A lock mass correction on the background ion $m/z = 445.12003$ was used. Precursors were dynamically excluded after $n = 1$ with an exclusion duration of 10 s and with a precursor range of 20 ppm. Included charge states were 2–5. For MS2 the first mass was set to 110 Da, and the MS2 scan resolution was 30,000 at an AGC target of 100% at a maximum fill time of 60 ms. Maxquant version 2.5.1.0 was used for label-free data processing with 10 ppm and 0.02 Da deviation for precursor and fragment mass, respectively. Trypsin was specified as the enzyme. Methionine oxidation and acetylation (on the protein N-terminus) were set as variable modifications. Carbamidomethyl was set as a fixed modification on cysteines. The false discovery rate was set at <1%. The full Maxquant database search parameters and output are available in the PRIDE submission PXD58087, also see data availability.

Bioinformatic analysis of DIA data. Peptide intensity table with the Label-free quantitation values was analyzed in Perseus (v1.6.2.3). Data were log2 transformed and filtered for identification in all three replicates in at least one group. PCA was performed for each analysis with default settings. Intensities were Z-scored by subtracting the mean and used for hierarchical clustering by Euclidean distance (preprocessed with k-means, 300 clusters, 1000 iterations). Missing values were imputed from the lower end of the normal distribution (default settings). A two-sided student's *t* test with permutation-based FDR was used to calculate the significance between treatment and control at 0.05 FDR (*p*-value). For a detailed protocol of data analysis in Perseus: https://cox-labs.github.io/coxdocs/interactions.html.

Bio layer interferometry (BLI)

DTX2 assay. Bio Layer Interferometry (BLI) measurements were conducted using an OctetRed system (ForteBio). Streptavidin-biosensors were equilibrated in buffer (25 mM Tris-Cl 100 mM NaCl, BSA (1 mg/mL), dextran (1 mg/mL), Tween 20 (0.05%) and DTT (1 mM) pH 7.5,) before loaded with Bt-ADPr-Ub[1], or the controls Bt-Ub (no ADPr), or Bt-ADPr (no Ub). The sensor tips were then transferred to solutions of DTX2 (ranging from 20 μM−0.163 μM) to assess the association rates of the analyte. Subsequently, the sensor tips were returned into buffer to reverse the ligand−protein interaction and estimate the corresponding dissociation rates. Dissociation constants (K_D) were then computed using the ForteBio Data Analysis software, employing simultaneous co-fitting of all concentrations.

RNF114 or RNF114 domain deletions assays. BLI measurements were conducted using an OctetRed system (ForteBio). Streptavidin-biosensors were equilibrated in buffer (50 mM HEPES, 50 mM NaCl, 5 mM $MgCl_2$, 1 mM DTT, BSA (1 mg/mL), dextran (1 mg/mL) and Tween 20 (0.05%), pH 7.5) before loaded with Bt-ADPr-Ub[1] or the controls Bt-Ub (no ADPr), or Bt-ADPr (no Ub). The sensor tips were then transferred to solutions of RNF114 or RNF114 domain deletions (ranging from 40 μM−0.83 μM) to assess the association rates of the analyte. Subsequently, the sensor tips were returned into buffer to reverse the ligand-protein interaction and estimate the corresponding dissociation rates. Dissociation constants (K_D) were then computed using the ForteBio Data Analysis software, employing simultaneous co-fitting of all concentrations.

Surface plasmon resonance assays (SPR)

All surface plasmon resonance (SPR) experiments were carried out on a Biacore T200 machine (GE Healthcare) at 25 °C. Biotinylated ligands −3′-ADPr-Ub[1], 3′-ADPr only[12] or Ub_{1-76} were immobilized (10-100 RU) on a streptavidin-coated sensor chip. Using a concentration series of the enzymes binding interactions of DTX2 or RNF114 with each ligand were assessed (separately) using 50 mM HEPES, pH 7.5, 50 mM NaCl, 5 mM $MgCl_2$, 1 mM DTT and 0.05% v/v Tween-20 supplemented with 1 mg/mL BSA and 1 mg/mL dextran as running buffer. Equilibrium dissociation constants (K_D) were determined by plotting steady-state equilibrium values against protein concentration and fitting these with 1:1 stoichiometry using the Biacore T200- and Prism (Graphpad) software.

In vitro conjugation assays with mass spectrometry read-out

To test the chain-building capacity and chain-building specificity of RNF114, an assay with neutron-encoded monoubiquitins was used[35]. In short, eight neutron-encoded monoubiquitin$_{1-75}$ acceptors (with only one available lysine position, all other lysines were mutated to arginine) were mixed in an equimolar amount (8× ~7.5 mM; 1.5× final concentration) together with donor mono ubiquitin$_{1-76}$ (all K-to-R) (60 μM; 1.5× final concentration). Recombinant purified conjugation enzymes were diluted to 10× final concentration (1 μM for UBE1, 25 μM for UBE2D1 enzyme and 50 μM for RNF114) in a buffer containing 20 mM Tris·HCl, 100 mM NaCl, pH 7.55 and 50 mM TCEP and $MgCl_2$. The monoUb mixture (6.33 μL) was added to an Eppendorf tube. Subsequently, the enzymes (1 μL E1, 1 μL E2 and 1 μL E3, 10× final concentration) were added to the monoUb mixture. The mixture was diluted with 0.7 μL buffer (20 mM Tris·HCl, 100 mM NaCl, pH 7.55 and 50 mM TCEP and $MgCl_2$). The reaction was started by the addition of 0.2 μL 0.5 M ATP. The reaction mixtures were incubated at 37 °C for 180 min. After 30 and 60 min fresh ATP (0.2 μL 0.5 M) was added to the solution. Before adding ATP, 1 μL of reaction mixture was taken for

timepoint 0 min. After 10, 30, 60, and 180 min a sample was taken from the reaction mixture for analysis. After the indicated incubation time, 1 µL of the reaction mixture was taken. The reaction was quenched by acidification of the mixture and internal standards for MS analysis were directly added. Samples were collected in a 96-well plate and measured by LC-MS analysis. 8 µL of the sample was injected onto the column. The samples were separated by an Acquity H-class UPLC system using a BEH C4 column (300 Å, 1.7 µM (2.1 × 100 mm)). Proteins were eluted using a shallow gradient that ranged from 29% up to 32% ACN in H_2O with 0.1% FA over 2 min using a flow rate of 0.6 mL/min, which was able to separate monoUb and diUb products (baseline level). Products were analysed by intact MS analysis on a XEVO G2 XS Q-TOF. The data were analysed using LaCyTools version 22.04.29. Data were aligned, quality control was performed (Mass Accuracy <15 ppm; IPQ < 0.25; $S/N > 9$) and the areas of all m/z peaks, within the quality control boundaries, from the same analyte were summed. The absolute area for each monoUb analyte was normalised at each timepoint using the non-processed K27 acceptor monoUb. The concentration of monoUb present at each timepoint was calculated using the theoretical concentration of present K27 acceptor monoUb in the analysed mixture. For the diUb signals, the total absolute areas under the curve for timepoint $t = 180$ min were summed, and the contribution per diUb to this total area was calculated as an indication of the relative amount of that specific diUb linkage type formed during the assay. Results were plotted using GraphPadPrism 10.2.3. (Code availability. LaCyTools is freely available for download at https://github.com/Tarskin/LaCyTools).

Imaging

Cell culture and live-cell imaging were completed as previously described[55]. Briefly, human U2OS osteosarcoma (American Type Culture Collection (ATCC), HTB-96) cells were cultured in Dulbecco's modified Eagle's medium (Sigma-Aldrich) supplemented with 10% fetal bovine serum (FBS; Gibco) and penicillin-streptomycin (100 U/ml; Gibco) in a humidified atmosphere at 37 °C with 5% CO_2. Cells were plated on an eight-well µ-slide glass bottom chamber slide (ibidi) and transfected with an expression plasmid for YFP-RNF114 WT, YFP-RNF114 UIM mutant (V220G,L221G,S224G), YFP-RNF114 ΔUIM (1-208), or ADPr binding mutants YFP-RNF114, Y186A, and C176A together with PaTagRFP-H2B using TransIT-LT1 Transfection Reagent (Mirus Bio), according to the manufacturer's instructions. The YFP plasmids were for either full-length RNF114 or ZnF2 + 3 + UIM truncation (140-C). Cells were incubated for 48 h prior to imaging. For cell sensitization before laser irradiation at 405 nm, growth medium was aspirated from the chamber slide and replaced with fresh medium containing Hoechst 33342 (0.3 µg/mL) for 1 h. Immediately before imaging, the Hoechst-containing medium was replaced with imaging media (phenol red−free Leibovitz's L-15 medium (Life Technologies) supplemented with 20% FBS, penicillin (100 µg/mL), and streptomycin (100 U/mL)). Live-cell microscopy was carried out on an Olympus IX-83 inverted microscope equipped with a Yokogawa SoRa super resolution spinning-disk head, a UPlanAop 60×/1.5 numerical aperture oil-immersion objective lens and a Prime BSI scientific complementary metal-oxide semiconductor camera. The fluorescence of YFP and PaTagRFP-H2B was excited with 488 nm and 561 nm solid-state lasers, respectively, and fluorescence detection was achieved with band-pass filters adapted to the fluorophore emission spectra. Laser microirradiation at 405 nm was performed along a 15 µm line through the nucleus for 250 ms using a single-point scanning head (Olympus cellFRAP) coupled to the epifluorescence backboard of the microscope. To ensure reproducibility, laser power at 405 nm was measured at the beginning of each experiment and set to 110 µW at the sample level. For time course experiments, images were collected every 5 s. For the live-cell imaging experiments, cells were maintained at 37 °C with a heating chamber. Protein accumulation at sites of damage (Ad) was then calculated as:

$$A_{damage} = \frac{I_{damage} - I_{background}}{I_{nucleus} - I_{background}} \quad (1)$$

The accumulated protein at the damage (Ad) is a measure of the intensity (I) at the sites of damage over the intensity of the entire nucleus, with subtracted background intensity. The intensity within the micro-irradiated area was then normalized to the intensity before damage induction. Photoactivated H2B was used as a reference to indicate where irradiation had occurred.

Statistical analysis

All statistical evaluations were reported on Student's t test (two-tailed distribution) having ns: not significant. All error bars correspond to the mean ± SD. Data were analyzed using the Microsoft Excel and GraphPad Prism5 software.

Reporting summary

Further information on research design is available in the Nature Portfolio Reporting Summary linked to this article.

Data availability

The mass spectrometry proteomics data have been deposited to the ProteomeXchange Consortium via the PRIDE partner repository with the dataset identifier PXD58087. The model is available in ModelArchive (www.modelarchive.org) with the accession code ma-gr42f [https://www.modelarchive.org/doi/10.5452/ma-gr42f]. All original Western Blots, SDS-PAGE analysis, BLI- and SPR-measurements, and detailed chemical synthesis protocols are available in the Supplementary information or in the Source data file. Source data are provided with this paper.

References

1. Pickart, C. M. Mechanisms underlying ubiquitination. *Annu. Rev. Biochem.* **70**, 503–533 (2001).
2. Cadwell, K. & Coscoy, L. Ubiquitination on nonlysine residues by a viral E3 ubiquitin ligase. *Science* **309**, 127–130 (2005).
3. Carvalho, A. F. et al. Ubiquitination of mammalian Pex5p, the peroxisomal import receptor. *J. Biol. Chem.* **282**, 31267–31272 (2007).
4. Wang, X. et al. Ubiquitination of serine, threonine, or lysine residues on the cytoplasmic tail can induce ERAD of MHC-I by viral E3 ligase mK3. *J. Cell Biol.* **177**, 613–624 (2007).
5. Pao, K. C. et al. Activity-based E3 ligase profiling uncovers an E3 ligase with esterification activity. *Nature* **556**, 381–385 (2018).
6. Kelsall, I. R., Zhang, J., Knebel, A., Arthur, J. S. C. & Cohen, P. The E3 ligase HOIL-1 catalyses ester bond formation between ubiquitin and components of the Myddosome in mammalian cells. *Proc. Natl. Acad. Sci. USA* **116**, 13293–13298 (2019).
7. Otten, E. G. et al. Ubiquitylation of lipopolysaccharide by RNF213 during bacterial infection. *Nature* **594**, 111–116 (2021).
8. Kelsall, I. R. et al. HOIL-1 ubiquitin ligase activity targets unbranched glucosaccharides and is required to prevent polyglucosan accumulation. *EMBO J.* **41**, e109700 (2022).
9. Sakamaki, J. I. et al. Ubiquitination of phosphatidylethanolamine in organellar membranes. *Mol. Cell* **82**, 3677–3692 e3611 (2022).
10. Zhu, K. et al. Ubiquitylation of nucleic acids by DELTEX ubiquitin E3 ligase DTX3L. *EMBO Rep.* **25**, 4172–4189 (2024).
11. Dearlove, E. L. et al. DTX3L ubiquitin ligase ubiquitinates single-stranded nucleic acids. *Elife* **13**, RP98070 (2024).
12. Zhu, K. et al. DELTEX E3 ligases ubiquitylate ADP-ribosyl modification on protein substrates. *Sci. Adv.* **8**, eadd4253 (2022).
13. Zhu, K. et al. DELTEX E3 ligases ubiquitylate ADP-ribosyl modification on nucleic acids. *Nucleic Acids Res.* **52**, 801–815 (2024).

14. Suskiewicz, M. J., Prokhorova, E., Rack, J. G. M. & Ahel, I. ADP-ribosylation from molecular mechanisms to therapeutic implications. *Cell* **186**, 4475–4495 (2023).
15. Groslambert, J., Prokhorova, E. & Ahel, I. ADP-ribosylation of DNA and RNA. *DNA Repair***105**, 103144 (2021).
16. Kang, H. C. et al. Iduna is a poly(ADP-ribose) (PAR)-dependent E3 ubiquitin ligase that regulates DNA damage. *Proc. Natl. Acad. Sci. USA* **108**, 14103–14108 (2011).
17. Zhang, Y. et al. RNF146 is a poly(ADP-ribose)-directed E3 ligase that regulates axin degradation and Wnt signalling. *Nat. Cell Biol.* **13**, 623–629 (2011).
18. Kar, P. et al. PARP14 and PARP9/DTX3L regulate interferon-induced ADP-ribosylation. *EMBO J.* **43**, 2929–2953 (2024).
19. Bhogaraju, S. et al. Phosphoribosylation of ubiquitin promotes serine ubiquitination and impairs conventional ubiquitination. *Cell* **167**, 1636–1649 e1613 (2016).
20. Yan, F. et al. Threonine ADP-ribosylation of ubiquitin by a bacterial effector family blocks host ubiquitination. *Mol. Cell* **78**, 641–652 e649 (2020).
21. Chatrin, C. et al. Structural insights into ADP-ribosylation of ubiquitin by Deltex family E3 ubiquitin ligases. *Sci. Adv.* **6**, eabc0418 (2020).
22. Yang, C.-S. et al. Ubiquitin modification by the E3 Ligase/ADP-ribosyltransferase Dtx3L/Parp9. *Mol. Cell* **66**, 503–516.e505 (2017).
23. Ahmed, S. F. et al. DELTEX2 C-terminal domain recognizes and recruits ADP-ribosylated proteins for ubiquitination. *Sci Adv* **6**, eabc0629 (2020).
24. Longarini, E. J. et al. Modular antibodies reveal DNA damage-induced mono-ADP-ribosylation as a second wave of PARP1 signaling. *Mol. Cell* **83**, 1743–1760 e1711 (2023).
25. Li, P. et al. Nimbolide targets RNF114 to induce the trapping of PARP1 and synthetic lethality in BRCA-mutated cancer. *Sci. Adv.* **9**, eadg7752 (2023).
26. Longarini, E. J. & Matic, I. Preserving ester-linked modifications reveals glutamate and aspartate mono-ADP-ribosylation by PARP1 and its reversal by PARG. *Nat. Commun.* **15**, 4239 (2024).
27. Tashiro, K. et al. Chemoenzymatic and synthetic approaches to investigate aspartate- and glutamate-ADP-ribosylation. *J. Am. Chem. Soc.* **145**, 14000–14009 (2023).
28. Liu, Q. et al. A general approach towards triazole-linked adenosine diphosphate ribosylated peptides and proteins. *Angew. Chem. Int. Ed.***57**, 1659–1662 (2018).
29. Gold, H. et al. Synthesis of sugar nucleotides by application of phosphoramidites. *J. Org. Chem.* **73**, 9458–9460 (2008).
30. Ismail, I. H. et al. The RNF138 E3 ligase displaces Ku to promote DNA end resection and regulate DNA repair pathway choice. *Nat. Cell Biol.* **17**, 1446–1457 (2015).
31. Rodriguez, M. S. et al. The RING ubiquitin E3 RNF114 interacts with A20 and modulates NF-kappaB activity and T-cell activation. *Cell Death Dis.* **5**, e1399 (2014).
32. Perrard, J. & Smith, S. Multiple E3 ligases control tankyrase stability and function. *Nat. Commun.* **14**, 7208 (2023).
33. Wang, Z. et al. Recognition of the iso-ADP-ribose moiety in poly(-ADP-ribose) by WWE domains suggests a general mechanism for poly(ADP-ribosyl)ation-dependent ubiquitination. *Genes Dev.* **26**, 235–240 (2012).
34. Kliza, K. W. et al. Reading ADP-ribosylation signaling using chemical biology and interaction proteomics. *Mol. Cell* **81**, 4552–4567 e4558 (2021).
35. Yang, Y. et al. The E3 ubiquitin ligase RNF114 and TAB1 degradation are required for maternal-to-zygotic transition. *EMBO Rep.* **18**, 205–216 (2017).
36. Capon, F. et al. Identification of ZNF313/RNF114 as a novel psoriasis susceptibility gene. *Hum. Mol. Genet.* **17**, 1938–1945 (2008).
37. van Tol, B. D. M. et al. Employing neuron-encoded monoUbs to study E2/E3 ligase activity and selectivity for assembling Ubiquitin chains. *bioRxiv*, 2025.05.22.655449 (2025).
38. Djerir, B. et al. An E3 ubiquitin ligase localization screen uncovers DTX2 as a novel ADP-ribosylation-dependent regulator of DNA double-strand break repair. *J. Biol. Chem.* **300**, 107545 (2024).
39. Ahel, I. et al. Poly(ADP-ribose)-binding zinc finger motifs in DNA repair/checkpoint proteins. *Nature* **451**, 81–85 (2008).
40. Eustermann, S. et al. Solution structures of the two PBZ domains from human APLF and their interaction with poly(ADP-ribose). *Nat. Struct. Mol. Biol.* **17**, 241–243 (2010).
41. Hurley, J. H., Lee, S. & Prag, G. Ubiquitin-binding domains. *Biochem J.* **399**, 361–372 (2006).
42. Sims, J. J. et al. Polyubiquitin-sensor proteins reveal localization and linkage-type dependence of cellular ubiquitin signaling. *Nat. Methods* **9**, 303–309 (2012).
43. Bejan, D. S., Lacoursiere, R. E., Pruneda, J. N. & Cohen, M. S. Ubiquitin is directly linked via an ester to protein-conjugated mono-ADP-ribose. *EMBO J.* **44**, 2211–2231 (2025).
44. V. De Cesare, et al, Deubiquitinating enzyme amino acid profiling reveals a class of ubiquitin esterases. *Proc. Natl. Acad. Sci. USA* **118**, e2006947118 (2021).
45. Spradlin, J. N. et al. Harnessing the anti-cancer natural product nimbolide for targeted protein degradation. *Nat. Chem. Biol.* **15**, 747–755 (2019).
46. Raja, R. et al. Interferon-induced PARP14-mediated ADP-ribosylation in p62 bodies requires an active ubiquitin-proteasome system. *EMBO J*, **44**, 2741–2773 (2024).
47. Lacoursiere, R. E. et al. A family of E3 ligases extend K11 polyubiquitin on sites of MARUbylation. bioRxiv 2025.05.11.653360; https://doi.org/10.1101/2025.05.11.653360 (2025).
48. Stokes, M. S. et al. NAD+ sensing by PARP7 regulates the C/EBPβ-dependent transcription program in adipose tissue in vivo. *bioRxiv*, https://doi.org/10.1101/2025.04.07.647692 (2025).
49. Perrard, J., Gao, K., Ring, K., Smith, S. Deltex and RING-UIM E3 ligases cooperate to create a ubiquitin-ADP-ribose hybrid mark on tankyrase, promoting its stabilization. *bioRxiv*, https://doi.org/10.1101/2025.04.09.648013 (2025).
50. Dietz, L. et al. Structural basis for SMAC-mediated antagonism of caspase inhibition by the giant ubiquitin ligase BIRC6. *Science* **379**, 1112–1117 (2023).
51. Jumper, J. et al. Highly accurate protein structure prediction with AlphaFold. *Nature* **596**, 583–589 (2021).
52. Mirdita, M. et al. ColabFold: making protein folding accessible to all. *Nat. Methods* **19**, 679–682 (2022).
53. Abramson, J. et al. Accurate structure prediction of biomolecular interactions with AlphaFold 3. *Nature* **630**, 493–500 (2024).
54. Elfmann, C. & Stulke, J. PAE viewer: a webserver for the interactive visualization of the predicted aligned error for multimer structure predictions and crosslinks. *Nucleic Acids Res.* **51**, W404–W410 (2023).
55. Dukic, N. et al. PARP14 is a PARP with both ADP-ribosyl transferase and hydrolase activities. *Sci. Adv.* **9**, eadi2687 (2023).

Acknowledgements

We would like to thank Alan Wainman and the Dunn School Bioimaging Facility for expert advice and access to the microscope. We also like to acknowledge Cami Talavera Ormeño and Robbert Kim from the LUMC peptide-facility and LUMC protein-facility for their help with peptide production and biophysical characterisation experiments, respectively. The work in I.A.'s laboratory is supported by the Wellcome Trust (223107 and 302632), Biotechnology and Biological Sciences Research Council (BB/R007195/1 and BB/W016613/1), Ovarian Cancer Research Alliance (813369), Oxford University Challenge Seed Fund (USCF 456), and Cancer Research United Kingdom (C35050/A22284). A.G. was

supported by the Sir Henry Wellcome Fellowship (Wellcome Trust, no. 224095/Z/21/Z). The work in the van der Heden van Noort laboratory is supported by the Dutch Research Council (NWO VIDI Grant, no. VI.Vidi.192.011) and the European Research Council (ERC CoG Grant, no. 101087582). The work in the Elliott laboratory is supported by UKRI BBSRC (BB/Y008936/1), UKRI MRC (MR/Z506217/1), and CRUK (DRCPFA-Jun24/100003).

Author contributions

The concept of this study was conceived by C.C., I.A., and G.J.v.d.H.v.N. Design and synthesis of probe **1** and BLI- and SPR-affinity measurements were performed by M.S.K. under supervision of G.J.v.d.H.v.N. Pull-down experiments were performed by R.M. and M.S.K. Proteomic measurements were performed by S.A.R., R.T.N.T. under supervision of P.A.v.V. Proteomic data analysis was performed by R.M. Profiling of RNF114 linkage selectivity was performed by B.D.M.v.T. Protein expression, initial discovery of the RNF114 enzymatic activity, biochemical characterisation and modelling was executed by C.C., K.Z., A.G., L.M., under supervision of P.R.E., D.A., and I.A. Experiments on recruitment of RNF114 (-mutants) to DNA damage induced sites were performed by R.S. The manuscript was prepared by M.S.K., C.C., I.A., and G.J.v.d.H.v.N. with input from all authors.

Competing interests

The authors declare no competing interests.

Additional information

Supplementary information The online version contains supplementary material available at https://doi.org/10.1038/s41467-025-61111-7.

Correspondence and requests for materials should be addressed to Chatrin Chatrin, Ivan Ahel or Gerbrand J. van der Heden van Noort.

Peer review information *Nature Communications* thanks Malte Gersch and the other, anonymous, reviewer(s) for their contribution to the peer review of this work. A peer review file is available.